ENSTA Bretagne · Ifremer
15ÈMES JOURNÉES DE L'HYDRODYNAMIQUE
22 - 24 novembre 2016 - Brest

MODÉLISATION DES EFFETS VISQUEUX DANS UN MODÈLE POTENTIEL DE VAGUES COMPLÈTEMENT NON-LINÉAIRE ET DISPERSIF

MODELING VISCOUS EFFECTS IN A FULLY NONLINEAR AND DISPERSIVE POTENTIAL WAVE MODEL

C. RAOULT[1,2], M. L. YATES[1,3], M. BENOIT[4], E. MONSALVE[5]
cecile.raoult@edf.fr, marissa.yates-michelin@cerema.fr, benoit@irphe.univ-mrs.fr, eduardo.monsalve@espci.fr

[1]Université Paris-Est, Laboratoire d'Hydraulique Saint-Venant (ENPC, EDF R&D, Cerema)
[2]EDF R&D, Laboratoire National d'Hydraulique et Environnement
[3]Cerema, Direction technique Eaux, mers et fleuves
[4]Institut de Recherche sur les Phénomènes Hors Equilibre (IRPHE), UMR 7342 (CNRS, Aix-Marseille Université, Ecole Centrale Marseille)
[5]Laboratoire de Physique et Mécanique des Milieux Hétérogènes PMMH, UMR CNRS 7636- ESPCI-UMPC Univ. Paris 6–UPD Univ., Paris 7

Résumé

Dans le but de modéliser les effets dissipatifs induits par la dissipation visqueuse interne et le frottement sur le fond affectant la propagation des vagues, les termes dissipatifs dérivés par Dias et al. [6] et Dutykh et Dias [8] sont ajoutés aux équations non-linéaires de Zakharov [23]. La condition d'imperméabilité sur le fond est modifiée pour rendre compte de la présence d'une couche limite au fond [14, 8]. Le modèle visco-potentiel résultant est présenté et validé par l'application à trois cas tests analytiques ou expérimentaux : (1) la décroissance d'une onde stationnaire linéaire, (2) l'atténuation d'une onde solitaire et (3) l'atténuation de vagues régulières se propageant sur une marche sous-marine. Les résultats des simulations montrent un bon accord avec la théorie pour l'atténuation de vagues en profondeur d'eau inifinie et finie, ainsi qu'un bon accord avec les mesures expérimentales.

Summary

With the objective of taking into account energy dissipation through bulk viscosity and bottom friction in a potential flow model, free surface dissipative terms derived by Dias et al. [6] and Dutykh and Dias [8] are added to the nonlinear Zakharov equations [23], and the impermeable bottom boundary condition is modified to take into account the presence of a boundary layer [14, 8]. The visco-potential flow model is presented and validated with the application of three analytic or experimental test cases: (1) decay of a linear standing wave, (2) attenuation of a solitary wave, and (3) attenuation of regular waves propagating over a submerged step. The simulation results agree well with the theory of wave attenuation in infinite and finite depth, as well as with the experimental measurements.

I – Introduction

Potential flow theory, which assumes an inviscid fluid and irrotational flow, often gives good results for water wave propagation modeling and is therefore a commonly used approach. However, it does not contain natural dissipation terms that may cause a decrease in the wave amplitude and a modification of the speed and shape of the waves in finite depth or over long propagation distances. Aside from wave breaking, three main processes lead to wave energy dissipation [13]: near-surface dissipation (caused by surface tension), internal dissipation by viscous stresses (or bulk viscosity), and interactions with solid boundaries (bottom and/or lateral wall friction). In intermediate and shallow water conditions, waves induce significant horizontal velocities near the bottom, and taking into account the effects of bottom friction becomes essential to reproduce correctly the wave characteristics and to study morphodynamics, including estimating accurately the bottom shear stress and the induced sediment transport fluxes.

Different theoretical estimations of wave damping have been derived depending on the dominant sources of energy dissipation: in infinite depth, only bulk viscosity is accounted for, whereas in finite depth, the effects of solid boundaries must also be considered. Lamb [11] derived the decay rate for a periodic wave of amplitude a in infinite depth for small values of viscosity. The amplitude decreases exponentially in time:

$$a(t) = a(t=0)\ e^{-2\nu k^2 t} \tag{1}$$

where k is the wave number and ν is the kinematic viscosity. Biesel [2] then derived an expression for wave damping in finite depth, and Hunt [9] added the effects of lateral walls in an experimental wave channel. More recently, Antuono and Colagrossi [1] derived a new approximation of the decay rate of gravity waves in a viscous fluid using the linearized Navier-Stokes equations, removing the assumption of infinite depth, and relaxing the assumption of small viscosity. In deep water and at first order, the obtained decay rate corresponds to that of Lamb [11]. However, the second-order term in the development is negative, showing that the first-order solution of Lamb [11] overestimates the decay rate. In finite depth, the differences are even more important since the solution of Lamb [11] does not consider dissipation by bottom friction.

Visco-potential models aim to take into account viscous effects without resolving the full Navier-Stokes equations by adding dissipative terms to the potential flow equations. With viscosity, corrective terms are added to the free surface boundary conditions to satisfy the new zero normal and tangential stress conditions [e.g. 6, 16, 10]. These solutions exhibit the same decay rate as Lamb [11] in the limit of long waves and small viscosity by taking into account the energy dissipation caused by bulk viscosity. Liu and Orfila [14] and Dutykh and Dias [8] additionally derived a new kinematic bottom boundary condition for the velocity potential with a non-local term in time using a boundary layer correction approach to take into account the effects of bottom friction (no-slip boundary condition). Boussinesq-type models have been derived from this new set of visco-potential equations [e.g. 12].

Here, the visco-potential equations are solved directly by restating them in terms of the boundary conditions to get a Zakharov-like set of equations taking into account bulk viscosity and bottom friction (described in part 2). Three analytical and experimental test cases are simulated with the derived numerical model including the attenuation of: (1) viscous standing waves [1], (2) a viscous solitary wave propagating over a flat bottom [15], and (3) regular waves propagating over a submerged step [18].

II – Model description

II – 1 Mathematical visco-potential flow model

Assuming irrotational flow of an inviscid and homogeneous fluid with constant density, potential flow theory is used. By additionally assuming a non-overturning free surface, the free surface boundary conditions can be rewritten as a function of the free surface position $\eta(\underline{x},t)$ and potential $\tilde{\Phi}(\underline{x},t) = \Phi(\underline{x},\eta(\underline{x},t),t)$, where $\underline{x} = (x,y)$, obtaining the Zakharov equations [23]. Here, these equations are supplemented with dissipative terms, modeling the dissipation due to bulk viscosity, following the work of Dias et al. [6] and Dutykh and Dias [8]. These terms are derived considering that vorticity has to be introduced in the model to verify the zero tangential stress condition at the free surface. These terms were derived assuming linear waves, but [6] conjectured these expressions could be used in the nonlinear model as well when the viscosity is small:

$$\frac{\partial \eta}{\partial t} = -\nabla_{\text{H}}\tilde{\Phi}.\nabla_{\text{H}}\eta + \tilde{w}(1+(\nabla_{\text{H}}\eta)^2) + 2\nu\Delta_{\text{H}}\eta, \tag{2}$$

$$\frac{\partial \tilde{\Phi}}{\partial t} = -g\eta - \frac{1}{2}(\nabla_{\text{H}}\tilde{\Phi})^2 + \frac{1}{2}\tilde{w}^2(1+(\nabla_{\text{H}}\eta)^2) - 2\,\nu\frac{\partial^2\Phi}{\partial z^2}, \tag{3}$$

where ∇_{H} and Δ_{H} are the horizontal gradient and Laplacian operators, respectively.

In shallow water, the predominant source of dissipation is bottom friction. By applying a no-slip condition at the bottom, the interior flow must be corrected to take into account the vertical rotational part of the velocity induced in the boundary layer [14, 8]. The impermeable boundary condition at the bottom (for a flat bottom, here) is replaced by:

$$\frac{\partial \Phi}{\partial z}(z=-h) = -\sqrt{\frac{\nu}{\pi}}\int_0^t \frac{\frac{\partial^2\Phi}{\partial z^2}(\underline{x},z=-h,\tau)}{\sqrt{t-\tau}}\,d\tau. \tag{4}$$

The influence of the viscosity is not instantaneous. The effect of the boundary layer is cumulative in time but weighted in favor of the current time.

II – 2 Numerical model

In this work, the model is limited to one horizontal dimension (i.e. $\underline{x} = x$). The numerical implementation, in a Fortran code called Misthyc, includes:

- high-order finite difference schemes to calculate horizontal spatial derivatives,
- an explicit four-step, fourth-order Runge-Kutta scheme (with a constant time step) to integrate in time,
- and a spectral method in the vertical (using a base of Chebyshev polynomials of maximum order N_T) following Tian and Sato [21] to solve the Laplace boundary value problem for the velocity potential in the entire domain.

For a more detailed description of the model, see Yates and Benoit [22] and Raoult et al. [20]. The time integral in the bottom boundary condition (Eq.(4)) is evaluated assuming that $\frac{\partial^2\Phi}{\partial z^2}(x,-h,\tau)$ is constant over each (small) time step Δt. The term $\frac{\partial^2\Phi}{\partial z^2}(x,-h,\tau)$ is

stored at each time step, for all the nodes of the domain, which may be computationally expensive in terms of both memory and CPU time if the domain is large and the integration time is long.

Additional complexities in implementing this term appear when there are relaxation zones for wave generation because the solution imposed in the relaxation zone does not take into account viscous effects. To avoid this problem, the viscous terms are applied outside of the relaxation zones, with a smooth transition to avoid a spatial discontinuity. However, when the bottom friction is large in shallow water or when high values of the viscosity are simulated, instabilities often develop at the end of the transition zone. The limit of stability depends on the water depth and the viscosity, and these values must be explored further.

III – Results

The visco-potential flow model is validated by applying it to three test cases: (1) a linear simulation to study the amplitude decay of a standing wave evolving over a flat bottom for two relative water depths, (2) a nonlinear simulation of laboratory measurements of the propagation of a solitary wave over a flat bottom, attenuated by bottom friction, and (3) a nonlinear simulation of the dissipation of regular waves propagating over a submerged step in small-scale experiments.

III – 1 Attenuation of a standing wave

The first test case consists of simulating linear standing waves that are dissipated due to the effects of bulk viscosity and bottom friction. Antuono and Colagrossi [1] (AC2013 hereafter) derived an accurate approximation of the damping rate from the linearized Navier-Stokes equations for waves propagating in finite depth in a viscous fluid for a wide range of Reynolds numbers. Here, simulations of standing waves with an amplitude $a = 0.05$ m, in constant depth $h = 1$ m are compared to the theoretical solution. The periodic domain is one wavelength long (L) and regularly discretized with $\Delta x = L/100$ and $N_T = 7$.

The temporal evolution of the total kinetic energy of the fluid is defined as:

$$E_c(t) = \frac{1}{2}\,\rho\left[\int_x \Phi(z=\eta,t)\;\frac{\partial\eta}{\partial t}(t)\;dx + \int_x \Phi(z=-h,t)\;\frac{\partial\Phi}{\partial z}(z=-h,t)\;dx\right], \qquad (5)$$

where the first term is the free surface contribution and the second term is the bottom contribution.

Two combinations of the viscosity (ν), or Reynolds number, $Re = h\sqrt{gh}/\nu$, and relative water depth (kh) are presented here (see Table 1). For each combination, two linear simulations were completed to evaluate the influence of bottom friction: one with only the bulk viscosity terms activated, and a second with both the bulk viscosity and bottom friction terms. For a given Reynolds number, the dissipation is expected to

Simulation	kh	$L(m)$	Re	ν (m^2/s)	Δx (m)	Δt (s)
1	π	2	500	0.006264	0.02 $(L/100)$	0.00567 $(T/200)$
2	$\pi/12$	24	500	0.06264	0.24 $(L/100)$	0.0775 $(T/100)$

Table 1: Non-dimensional, physical and numerical parameters for the two simulations.

increase when the relative water depth decreases and when the bottom friction term becomes increasingly dominant.

In some cases, small wavelength oscillations in the free surface elevation appear when the bottom friction term is applied. The simulations were stabilized by applying a low-pass filter to the variable $\frac{\partial^2 \Phi}{\partial z^2}(x, z = -h)$, retaining only the first ten Fourier modes.

In deep water conditions ($kh = \pi$), the effects of bottom friction are negligible, and the simulation results with and without bottom friction are superimposed (Figure 1a). The decay rate derived by Lamb [11] overestimates the energy dissipation in comparison to the solution proposed by AC2013, in particular for small Reynolds numbers (high viscosity). As previously stated, Lamb's theory overestimates the damping rate obtained by AC2013 because of the existence of negative higher order terms in AC2013's solution. The simulation results agree well with Lamb's theory since the bulk viscous terms were derived using the same small viscosity assumption to neglect terms of order o(ν).

In the shallow water limit, the differences between the simulations with and without bottom friction become significant (Figure 1b). The damping increases with bottom friction, causing a decrease in the wave amplitude and propagation speed, as seen by the phase shift between the curves. The simulation that includes only the effects of bulk viscosity again agrees well with Lamb's theory, while the simulation that also includes bottom friction agrees well with the solution proposed by AC2013. For small relative water depths, the bottom friction term contributes significantly to wave dissipation and cannot be neglected to reproduce correctly the amplitude decay of the standing wave.

III – 2 Amplitude decay of a solitary wave

The second test case simulates the propagation of a solitary wave over a flat bottom ($h_0 = 0.15$ m), following the experiments of Liu et al. [15]. In the experiments, the wave is generated by a piston-type wavemaker, propagates over a flat bottom, and then shoals on a slope. Acoustic gauges in the wave flume record the evolution of the free surface elevation in the flat-bottom zone and in the shoaling zone (black triangles in Figure 2). The numerical simulations examine the flat-bottom zone, in a domain extending from $x = 0$ m to $x = 25$ m (slope beginning at $x = 19.88$ m), with a regular mesh ($\Delta x = 0.0075$ m), and $N_T = 7$. Since the numerical model is not able to simulate run-up at the waterline, a minimal depth ($h_1 = 0.01$ m) is set, and the simulations are stopped before the wave arrives at the reflective right boundary.

The initial condition is a solution of the fully nonlinear Euler equations for a solitary wave, computed with the algorithm of Clamond and Dutykh [3] for the solitary wave amplitude measured at the first gauge ($x = 6.5$ m). The smallest ($a = 0.01365$ m) and largest ($a = 0.06135$ m) wave amplitudes tested by [15] are simulated here (Table 2).

These nonlinear simulations take into account the effects of bulk viscosity using the viscous correction terms derived following linear theory. Dias et al. [6] hypothesized that these terms can be generalized to the fully nonlinear equations, and this hypothesis is

a (m)	ϵ	Δt (s)	CFL
0.01365	0.091	0.006	1
0.06135	0.409	0.0052	1

Table 2: Parameters for the two simulations of the solitary wave, showing the wave amplitude a, wave steepness $\epsilon = a/h$, time step Δt, and CFL number, defined as $CFL = C\Delta t/\Delta x$ (with C given by the algorithm of Clamond and Dutykh [3]).

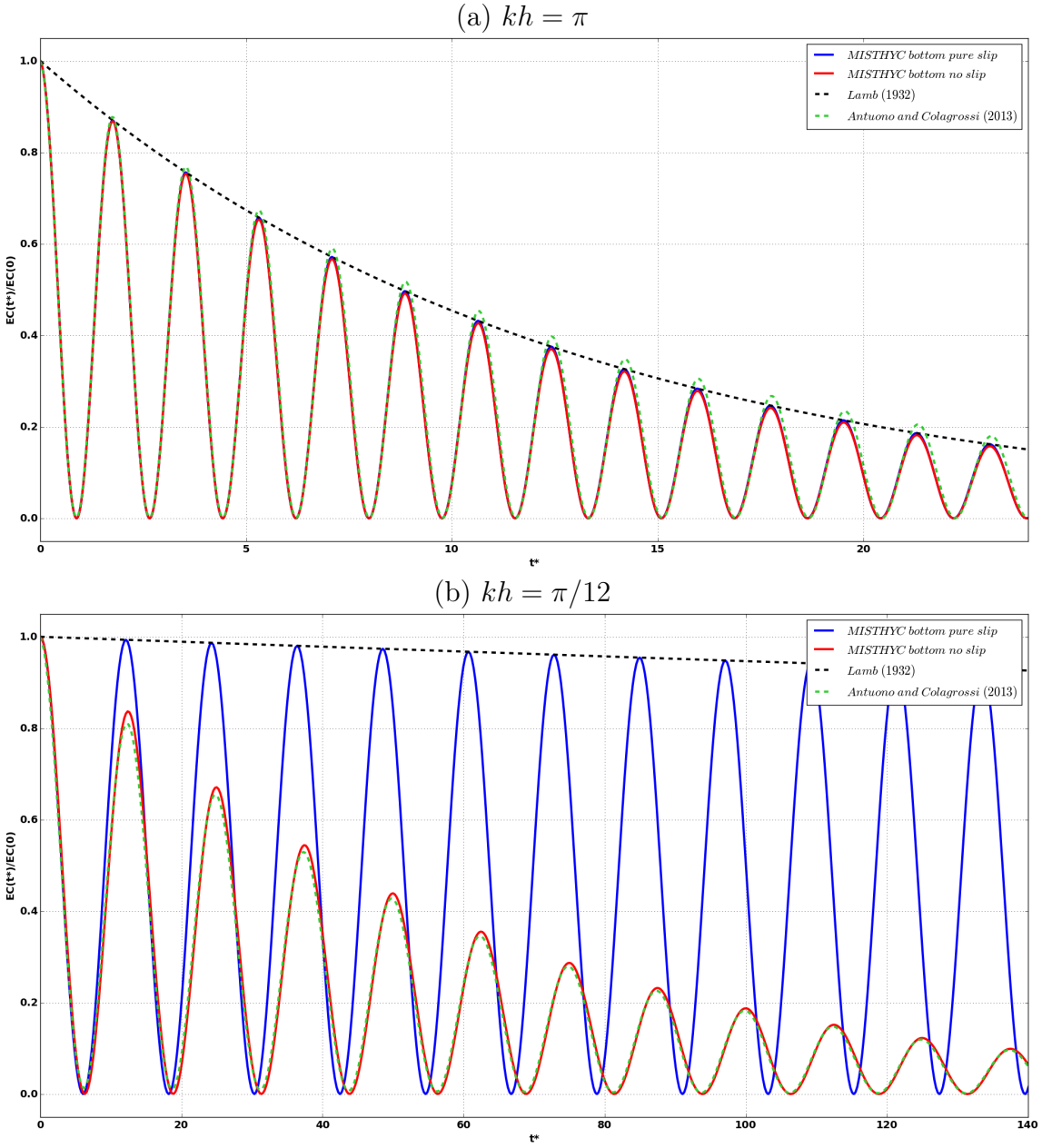

Figure 1: Evolution of the normalized kinetic energy of the system (Eq.(5)) as a function of nondimensional time ($t^* = t\sqrt{g/h}$) for $Re = 500$ ($\nu = 0.006264\ m^2/s$), and relative depths (a) $kh = \pi$ (deep water) and (b) $kh = \pi/12$ (shallow water).

tested here by comparing the propagation of solitary waves with small ($\epsilon = 0.091$) and then non-negligible ($\epsilon = 0.409$) nonlinearities ($\epsilon = a/h$).

In the flat-bottom region, the amplitude of the solitary wave decreases due to the combined effects of dissipation by bulk viscosity and bottom friction (Figure 3). The influence of the different sources of energy dissipation on the decay rate is shown in Figure 3. Without viscosity ($\nu = 0\ m^2/s$), the wave amplitude remains constant. The simulations with only the bulk viscosity terms added (slip bottom condition), with $\nu = 7.10^{-6}\ m^2/s$, show only a weak amplitude decay and are nearly superimposed on the simulations without viscosity. When the bottom friction term is added (no-slip bottom condition), the solitary wave amplitudes decrease significantly. This effect is more pronounced for larger wave heights that induce larger horizontal velocities at the bottom.

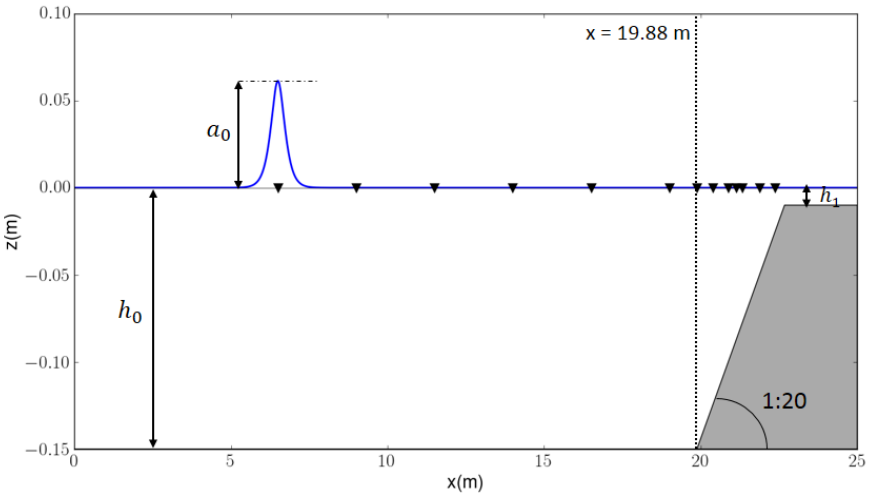

Figure 2: Bathymetry, initial free surface elevation, and positions of wave gauges (triangles) in the Liu et al. [15] experiments.

The value of the viscosity required to best fit the experimental data ($\nu = 7.10^{-6}\ m^2/s$, black line, Figure 3) is slightly higher than the kinematic viscosity of water ($\nu = 10^{-6}\ m^2/s$, dark blue line, Figure 3). Using a Boussineq model to simulate these experiments, Liu et al. [15] reproduced the decay rate of the experiments with a viscosity of $10^{-6}\ m^2/s$ when taking into account the effects of the boundary layers on the wave flume walls. Here the dissipation from the lateral walls is not taken into account, which likely explains the improvement in the comparison to the experiments when a larger value of the viscosity is simulated. The same optimal value of viscosity ($\nu = 7.10^{-6}\ m^2/s$) is used in the simulations for both wave heights, showing the insensitivity of the dissipation term to the wave non-linearity for these wave conditions.

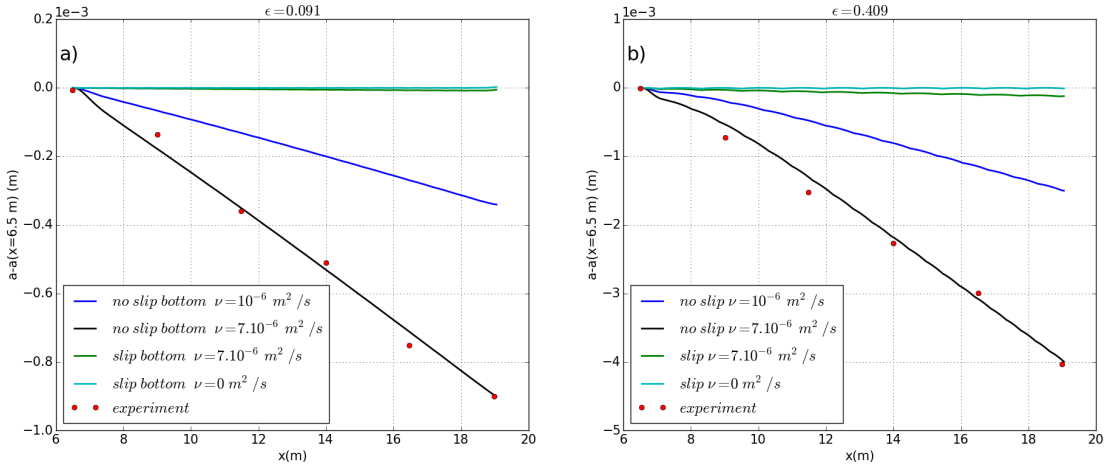

Figure 3: Decrease in the solitary wave amplitude along the wave flume for (a) $\epsilon = 0.091$ and (b) $\epsilon = 0.409$, showing the experimental data (red circles) and the numerical results without viscosity, $\nu = 0\ m^2/s$ (light blue line), with $\nu = 10^{-6}\ m^2/s$ pure slip bottom condition (green line), with $\nu = 10^{-6}\ m^2/s$ no-slip bottom condition (dark blue line), and with $\nu = 7.10^{-6}\ m^2/s$ no-slip bottom condition (black line) .

III – 3 Attenuation of regular waves propagating over a step

The last test case also uses the nonlinear version of the model to simulate the propagation of regular waves over a vertical submerged step, based on the small-scale experiments performed by E. Monsalve at the ESPCI (Ecole Supérieure de Physique et de Chimie Industrielle de la ville de Paris) [18]. The goal of this test is to study the generation, propagation, and dissipation of high-order harmonics over a step, in particular focusing on the second harmonic. The domain is divided into two zones: zone (I), the deeper region, and zone (II), the shallower region over the step. The subscripts $(I), (II)$ will be used to represent the wave and water depth characteristics in the two zones. The second harmonic can be decomposed into two components: (1) bound waves that propagate at the same celerity as the fundamental mode, with frequency $2f_1$ and wave number twice the fundamental wave number ($2k_1^{(II)} = 2k(f_1, h^{(II)})$), and (2) free waves with the wave number corresponding to the linear dispersion relation for the frequency $2f_1$ ($k_2^{(II)} = k(2f_1, h^{(II)})$) that propagate at the corresponding celerity. These two components interact, causing a spatial modulation of the second harmonic amplitude with a beat length [17]:

$$D^- = \frac{2\pi}{k_2^{(II)} - 2k_1^{(II)}} \tag{6}$$

In the experiments, waves are generated by a flap wavemaker, and strong nonlinearities are created at the vertical step at $x = 0$ m, transitioning between the deep water region ($h^{(I)} = 6.5$ cm) and the shallow water region ($h^{(II)} = 2.0$ cm). At the right end of the domain (from $x = 0.85$ m), an absorbing beach of slope 8% is constructed to prevent wave reflection. The free surface deformation is measured with high spatial and temporal resolution using a non-intrusive method, called Fourier Transform Profilometry [4].

In the numerical model, the vertical step is modeled with a hyperbolic tangent, with a transition of slope 85 degrees to avoid creating a discontinuity at the step (see inset in Figure 4). The numerical domain is the same as the experimental domain ($x \in [-0.38\ m;\ 0.85\ m]$), with the addition of a L_{gen}-wide relaxation zone for wave generation and a L_{abs}-wide relaxation zone for wave absorption (Figure 4). The width of the relaxation zones are $L_{gen} = L_1^{(I)}$ and $L_{abs} = 2L_1^{(II)}$. Waves are generated with a Dirichlet boundary condition for the potential computed using linear wave theory. The amplitude of the incident wave was not measured in the experiments (only the motion of the wave maker was prescribed), so a wave amplitude was determined to fit qualitatively the experimental data before the step. For an incident wave frequency of $f_1 = 1.9837$ Hz, the wave amplitude is estimated to be $a = 3.2$ mm, and wavelength (from the linear dispersion relation) is $L_1^{(I)} = 0.334$ m in depth $h^{(I)}$ and $L_1^{(II)} = 0.2112$ m in depth $h^{(II)}$. The domain was irregularly meshed with $\Delta x = L_1^{(I)}/100$ far from the step and a refinement of $\Delta x/2$ near the step, with $N_T = 7$. The time step is $\Delta t = 0.025$ s $\approx T_1/200$ for a maximum CFL=1.

For these small-scale experiments, the impacts of surface tension are important because surface tension (σ) modifies the linear dispersion relation [7]:

$$\omega^2 = \left(1 + \frac{1}{Bo}\right) gk \tanh(kh), \tag{7}$$

where $Bo = \rho g/(\sigma k^2)$ is the Bond number quantifying the ratio between gravity effects and surface tension effets. If $Bo \gg 1$, surface tension effects can be neglected. The beat

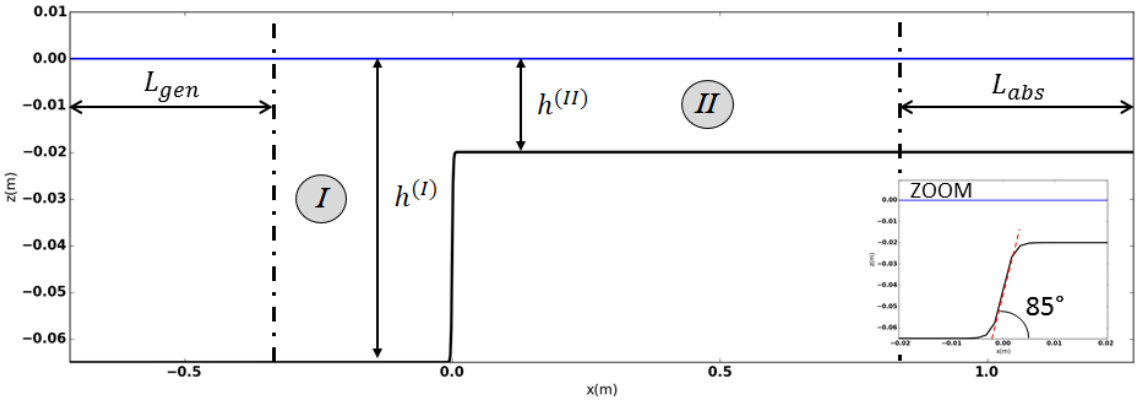

Figure 4: Numerical model domain and bathymetry for the submerged step test case. The inset shows a zoom of the hyperbolic tangent form of the step transition in the bottom elevation.

length of the second harmonic is expressed as a function of the difference between the wave numbers of the free and bound components (Eq.(6)). In the shallow region over the step (in water depth $h^{(II)}$), the Bond numbers corresponding to $k_1^{(II)}$ and $k_2^{(II)}$ are $Bo = 158$ and $Bo = 29$, respectively (Table 3). Surface tension impacts short waves with wavelengths on the order of centimeters, and the wave lengths associated with the second harmonic over the step are less than 10 cm. The influence of surface tension on their associated wavelength is small (Table 3), but important enough to modify the beat length.

To take into account the effects of surface tension in the numerical model, the dynamic free surface boundary condition (1DH version of Eq.(3)) is modified with a term proportional to the curvature of the free surface [e.g. 5]:

$$\frac{\partial \tilde{\Phi}}{\partial t} = -g\eta - \frac{1}{2}\left(\frac{\partial \tilde{\Phi}}{\partial x}\right)^2 + \frac{1}{2}\tilde{w}^2\left(1 + \left(\frac{\partial \eta}{\partial x}\right)^2\right) - 2\,\nu\frac{\partial^2 \Phi}{\partial z^2} + \frac{\sigma}{\rho}\frac{\partial}{\partial x}\left(\frac{\frac{\partial \eta}{\partial x}}{\sqrt{1 + \left(\frac{\partial \eta}{\partial x}\right)^2}}\right). \quad (8)$$

These nonlinear simulations take into account the effects of bulk viscosity and surface tension ($\sigma = 0.071\ N/m$). To compare the simulations to the experimental data, the free surface elevation time series are decomposed into the amplitudes of the first five harmonics (Figure 5). The optimal value of the bulk viscosity ν was sought to reproduce the amplitude of the second harmonic (Figure 5). The optimal value $\nu = 4.10^{-5}\ m^2/s$ is higher than viscosity of pure water, likely due to the fact that only bulk dissipation is simulated, whereas the effects of bottom friction may be important.

By including the effects of surface tension and bulk viscosity, the model reproduced well the generation of higher order harmonics on the step, the second harmonic beat length,

σ (N/m)	$k_1^{(II)}$ (rad/m)	$L_1^{(II)}$ (m)	$k_2^{(II)}$ (rad/m)	$L_2^{(II)}$ (m)	D^- (m)
0	29.65	0.2118	70.95	0.08855	0.5393
0.071	29.54	0.2127	69.11	0.09090	0.6264

Table 3: Wave number and wavelength of the first and second harmonics with the associated beat length for the water depth $h^{(II)} = 2.0$ cm, and for surface tension $\sigma = 0$ N/m and $\sigma = 0.071$ N/m.

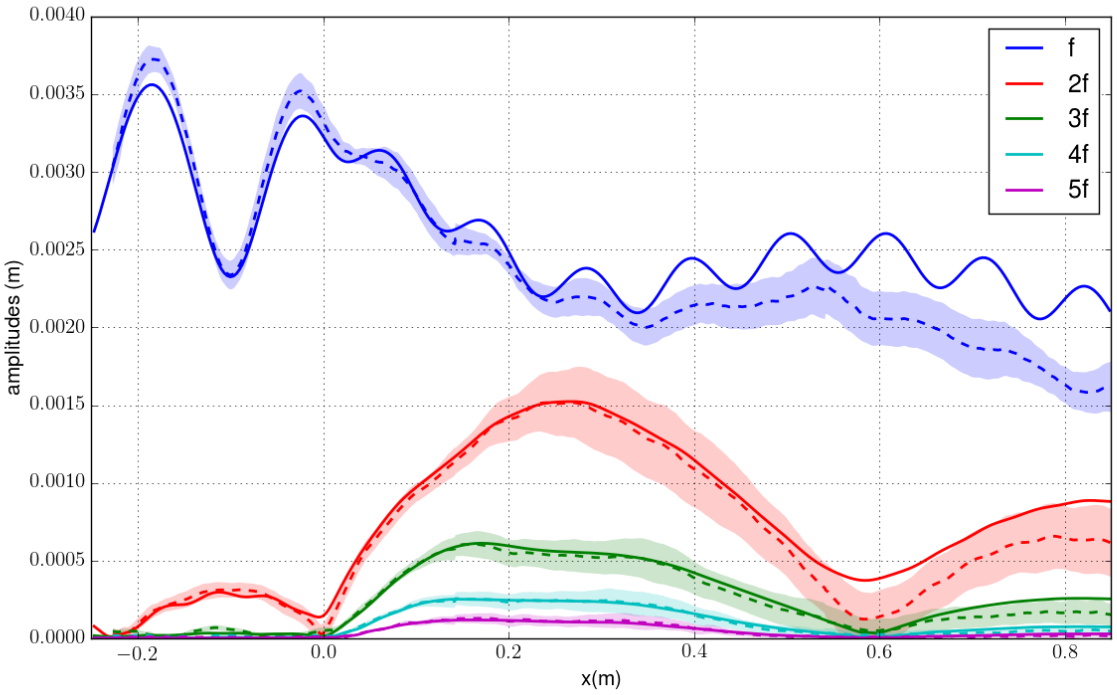

Figure 5: Simulated (solid line) and measured (dashed line) spatial evolution of the first five harmonic amplitudes for $f_1 = 1.9837$ Hz (using viscosity $\nu = 4.10^{-5}\ m^2/s$ and surface tension $\sigma = 0.071\ N/m$ in the simulation). The experimental data is averaged across the wave channel to compare to the 1DH simulations, and the colored shaded zones indicate the standard deviation of the measurements.

and, in general, the observed amplitude dissipation (Figure 5). However, the simulations still slightly overestimate the observed decay in amplitude of the first harmonic, even with an optimal viscosity $\nu = 4.10^{-5}\ m^2/s$ greater than that of pure water.

Bottom friction may have an important role in the dissipation of low frequency waves in shallow water. Taking into account the effects of bottom friction may correct the overestimation of the viscosity and improve the agreement with the experiments. Therefore, the bottom friction term was applied in the numerical model in the entire domain outside of the wave generation zone. However, this did not give satisfactory results in the region around the vertical step since the bottom friction term was derived assuming a flat bottom. Therefore, the no-slip condition was applied only in the shallow water region. To prevent a discontinuity in the bottom boundary condition, the viscosity in the bottom friction term was gradually increased in space to the target value. With the optimal value of viscosity required to reproduce the amplitude decay in the experiments, numerical instabilities eventually appear in the viscosity transition zone. Therefore, only simulations taking into account the effects of bulk dissipation are shown here.

Finally, the high wave dissipation observed in the experiments may also be an artifact of the experimental procedure that requires a perfectly clean free surface to avoid additional wave damping (from interactions between capillary-gravity waves and Marangoni waves that develop on the surface film, see Przadka et al. [19]).

Additional simulations at a range of wave frequencies (not shown here) demonstrated that the optimal value of the bulk viscosity must be adapted for each frequency. Overall, the model reproduces well the experimental data, including the generation of high-order harmonics and their subsequent evolution and attenuation due to bulk viscosity effects.

IV – Conclusions

Viscous dissipation was introduced in a nonlinear potential flow model deriving a visco-potential system of equations that contains: (1) two additional terms in the free surface boundary conditions to take into account the predominant contribution of the vortical component of the velocity, (2) the modification of the bottom boundary condition to take into account the presence of a boundary layer. The linear version of the visco-potential model reproduces well the decay of a linear standing wave, in comparison to the analytical solution of [11] for infinite depth and [1] for finite depth. In addition, simulations with the nonlinear version of the model agree well with experimental measurements of the decay of a solitary wave propagating over a flat bottom and the propagation and decay of higher-order harmonics generated at a nearly vertical step. Current work focuses on the numerical implementation of the bottom friction term, in particular for variable bottom.

V – Acknowledgements

The authors thank A. Maurel, P. Petitjeans, and V. Pagneux for sharing their experimental data and for participating in numerous discussions concerning the comparison of the numerical simulations and experimental observations. The authors would also like to thank Sébastien Boyaval and Jeffrey Harris for their enlightening discussions concerning visco-potential models.

References

[1] M. Antuono and A. Colagrossi. The damping of viscous gravity waves. *Wave Motion*, 50:197–209, 2013.

[2] F. Biesel. Calcul de l'amortissement d'une houle dans un liquide visqueux de profondeur finie. *La Houille Blanche*, 4:630–634, 1949.

[3] D. Clamond and D. Dutykh. Fast accurate computation of the fully non linear solitary surface gravity waves. *Computers & Fluids*, 84:35–38, 2013.

[4] P.J. Cobelli, A. Maurel, V. Pagneux, and P. Petitjeans. Global measurement of water waves by Fourier Transform Profilometry. *Exp. Fluids*, 46:1037–1047, 2009.

[5] F. Dias and C. Kharif. Nonlinear gravity and capilary-gravity waves. *Annu. Rev. Fluid Mech.*, 31:301–347, 1999.

[6] F. Dias, A.I. Dyachenko, and V.E. Zakharov. Theory of weakly damped free-surface flows: A new formulation based on potential flow solutions. *Physics Letters*, A 372: 1297–1302, 2008.

[7] M. W. Dingemans. *Water wave propagation over uneven bottom*, volume 13. World Scientific Publishing, 1997.

[8] D. Dutykh and F. Dias. Viscous potential free-surface flows in a fluid layer of finite depth. *C.R. Acad. Sci. Paris*, 345:113–118, 2007.

[9] J.N. Hunt. Viscous damping of waves over an inclined bed in a channel of finite width. *La Houille Blanche*, 7:836–842, 1952.

[10] D.D. Joseph and J. Wang. The dissipation approximation and viscous potential flow. *J. Fluid Mech.*, 505:365–377, 2004.

[11] H. Lamb. *Hydrodynamics*. Cambridge University Press, 1932.

[12] H.V.J. Le Meur. Derivation of a viscous Boussinesq system for surface water waves. *Asymptotic Analysis*, 94:309–345, 2015.

[13] J. Lighthill. *Waves in Fluids*. Cambridge University Press, 1978.

[14] P.L.-F. Liu and A. Orfila. Viscous effects on transient long-wave propagation. *J. Fluid Mech.*, 50:83–92, 2004.

[15] P.L.-F. Liu, G. Simarro, and A. Orfila. Experimental and numerical investigation of viscous effects on solitary wave propagation in a wave tank. *Coastal Eng.*, 53: 181–190, 2006.

[16] M.S. Longuet-Higgins. Theory of weakly damped Stokes waves: a new formulation and its physical interpretation. *J. Fluid Mech.*, 235:319–324, 1992.

[17] S.R. Massel. Harmonic generation by waves propagating over a submerged step. *Coastal Eng.*, 7:357–380, 1983.

[18] E. Monsalve, A. Maurel, V. Pagneux, and P. Petitjeans. Propagation of nonlinear waves passing over submerged step. *Physics Procedia*, 70:863–866, 2015.

[19] A. Przadka, B. Cabane, V. Pagneux, A. Maurel, and P. Petitjeans. Fourier transform profilometry for water waves: how to achieve clean water attenuation with diffusive reflection at the water surface? *Exp. Fluids*, 52:519–527, 2015.

[20] C. Raoult, M. Benoit, and M.L. Yates. Validation of a fully nonlinear and dispersive wave model with laboratory non-breaking experiments. *Coastal Eng.*, 114:194–207, 2016.

[21] Y. Tian and S. Sato. A numerical model on the interaction between nearshore nonlinear waves and strong currents. *Coast. Eng. Journal*, 50(4):369–395, 2008.

[22] M.L. Yates and M. Benoit. Accuracy and efficiency of two numerical methods of solving the potential flow problem for highly nonlinear and dispersive water waves. *Int. J. Numer. Methods Fluids*, 77:616–640, 2015.

[23] V. E. Zakharov. Stability of periodic waves of finite amplitude on the surface of a deep fluid. *J. Appl. Mech. Tech. Phys.*, 9(2):190–194, 1968.